Inertial waves in the Ibiza Channel

J. García Lafuente [a], N.C. Lucaya [b]

[a] *Department of Physics, University of Málaga, Spain*
[b] *Laboratorio Costero, Instituto Español de Oceanografía (IEO), Málaga, Spain*

Abstract

Currentmeter data taken in the Ibiza Channel show the almost permanent presence of near-inertial motions below the mixed layer. They correspond to downwards progressing waves with a vertical group velocity of some m/day. The presence of the Balearic Front sensibly affects the propagation of these inertial waves. Although situations exist in which the passage of atmospheric fronts along the Channel is clearly the generating force of these near-inertial motions we find others in which the energy density in mid-depths is higher than in any other depth. These last situations are closely related to the arrival to the Channel of some of the different water masses which flow around there. A clear correspondence between the presence of relatively strong inertial waves and a noticeable vertical shear of the subinertial flow, evidenced by an averaged Richardson number, is also observed. In some circumstances, the vertical shear of the whole flow (inertial plus subinertial) is higher than the stability limit, that is, $Ri < 0.25$, favoring the breaking of the internal waves. This could be a plausible cause of their decay and a reason to explain why they do not penetrate further than certain depths.

1. Introduction

Although motions of frequency proximate to the local inertial frequency, f, are detected in every depth of the ocean, they are more energetic in the surface mixed layer. Here, they are generated by the wind stress. D'Assaro (1985) makes a classification of the atmospheric features that produce "inertial events" in the mixed layer evaluating the flux of energy from wind into inertial motions associated to each of those. Although large stationary low pressure systems or steady zonal jets may produce strong wind stress on the sea surface, these features do not excite inertial oscillations. Small scale features [O(100 km)], as fronts or small lows, being advected at the typical speed of atmospheric systems [O(10 m/s)] will produce a time fluctuating wind of scale $1/f$ at a

given location and, consequently, they are very effective in generating inertial motions. The convergence/divergence of the generated currents in the mixed layer induces vertical motion of inertial period at the base of the layer ("inertial pumping" as named by Gill, 1984) and isopycnals below it. These oscillations establish the pressure gradients into the interior of the ocean which are necessary for the downwards propagation of the waves. They do it as a set of baroclinic modes with frequencies slightly greater than f. Their horizontal propagation speeds are quite less than those of the atmospheric fronts which produce them and their vertical group velocity, c_{gz}, is of the order of m/day (Gill, 1984; Kundu and Thomson, 1985).

The above description suggests horizontal coherence scales of the same order of the typical

lengths of the mesoscale atmospheric phenomena which generate the waves. However, the presence of oceanic fronts drastically reduces this scale to some tens of km (Kunze and Sanford, 1984; Weller, 1985; Rubinstein and Roberts, 1986; Eriksen, 1988). These fronts affect the propagation of the near-inertial waves that now could be trapped horizontally in troughs of negative relative vorticity of the fronts, or resulting in critical layers in the vertical (Kunze, 1985). The concurrence in time of the passage of an atmospheric front and the presence of an oceanic front in the neighbourhood of the mooring site could induce to the appearance of abnormally intense waves in great depths (Weller et al., 1991). Moreover, coastal boundaries will play an important role not only in generating these waves but in limiting their length-scale in enclosed seas as the Mediterranean.

Many of the peculiarities and characteristics mentioned are recognised in the current meter records taken in the Ibiza Channel between November, 1990 and July, 1991. Before commenting on these results, we find it necessary to make a brief oceanographic description of this channel.

2. Oceanographic characteristics

The name "channel" for the region under study (see Fig. 1) is somewhat confusing; neither the width/length ratio (greater than unity) nor that of depth/width describes the usual picture of a channel. The external radius of deformation ($R_o \approx 700$ km for a mean depth of 400 m) is greater than its width (≈ 90 km) the internal ones, much shorter. If we resolve the standard Sturm–Liouville problem to perform the expan-
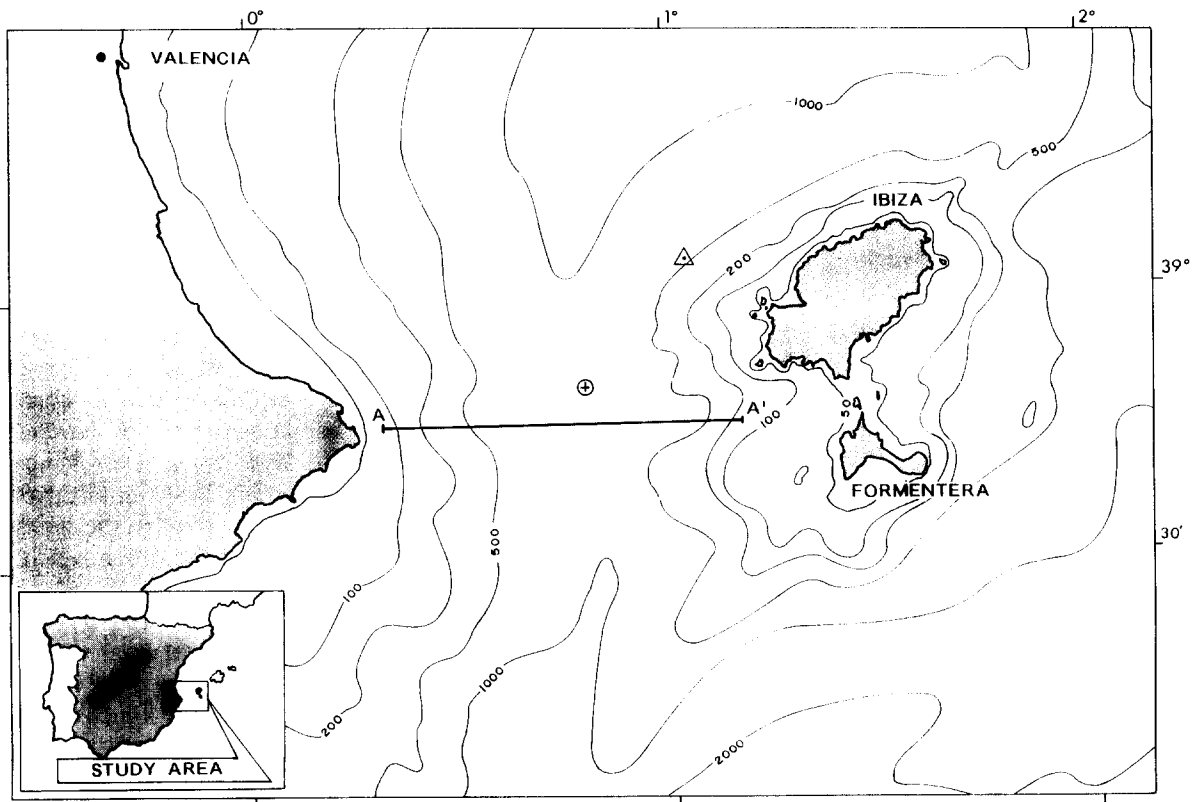

Fig. 1. Map of the area of study. Symbol $\oplus$ indicates the mooring position and Δ, the place where wind data are available. Line AA' is the transect whose vertical section is shown in Fig. 2.

sion in vertical modes for the profile of $N(z)$ in Fig. 6, we obtain $c_1 = 0.51$ m/s for the first baroclinic mode and 5.6 km for the internal radius (local inertial frequency $f = 9.11 \cdot 10^{-5}$ s^{-1} $= 0.0522$ c/h). Thus, the combined effects of rotation and stratification are important. Because of its dimensions it could contain and even generate mesoscale eddies (Fig. 2b). However, other details such as the existence of a sill, or by connecting regions with different oceanographic characteristics, e.g. the Gulf of Leon, where Western Mediterranean Deep Water (WMDW) is formed and the Algerian Basin, connected to the Alboran Sea and the Strait of Gibraltar where the water of the Mediterranean Sea is renewed, do reflect the image of a channel.

Four different water masses can be found there (Lopez Jurado et al., 1992): Modified Atlantic Water (MAW), relatively warm and fresh and flowing northwards preferably on the eastern side of the Channel; Levantine Intermediate Water (LIW), the saltiest, which flows south in the direction of the Strait of Gibraltar; Western Mediterranean Intermediate Water (WMIW), the coldest, with seasonal characteristics, formed locally at the coast to the north of the Ibiza Channel in winter and the WMDW already mentioned, the most dense, which cannot be detected if it lays at a greater depth than the sill of the Channel.

The encounter of waters flowing south coming from the Catalan Sea with those of Atlantic origin (MAW) that moves northwards forms the so-called Balearic Front (Font, 1986), which is often displayed both by satellite imagery (La Violette et al., 1990; Lopez, 1991; Levovrh et al., 1992), or hydrographic sections (Fig. 2).

Mesoscale instabilities can be associated with this front (Wang et al., 1988) as well as fluctuations in its position (La Violette et al., 1990)
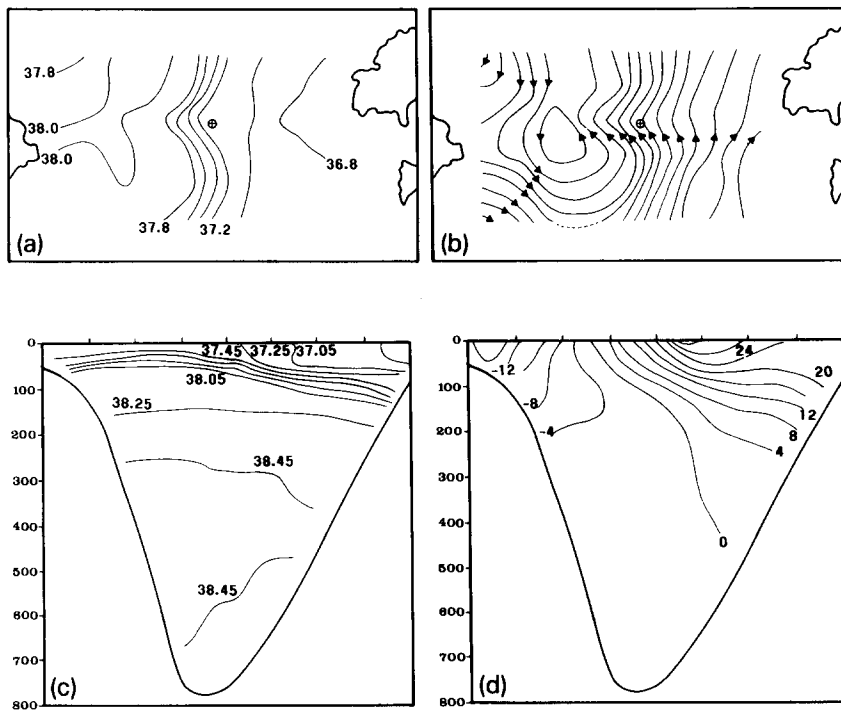

Fig. 2.(a) Distribution of salinity (PSU) at 50 m depth in November, 1990. (b) Dynamic height anomaly of the sea surface with reference to 600 db (interval: 1 cm dyn). In both, the mooring site has been shown. (c) Vertical distribution of salinity in the AA′ transect. (d) Idem of geostrophic velocity with positive values indicating flow towards the north. All these figures show the presence of a frontal structure near to the mooring site.

Table 1
Summary of the data used in this study

	(A) Currentmeter data		
Part	Location	Depths (m)	From-to
1	38°49,4′N/0°48,0′E	90, 115, 165, 265, 465, 715	15/11/90-15/3/91
2	38°49,3′N/0°48,1′E	100, 125, 200, 250, 450, 700	20/3/91-24/7/91
	(B) Meteorological data		
Variable	Location		From-to
Geostrophic winds	39°9,6′N; 1°4,3′E		1/11/90-25/7/91
Mean pressure	41°N, 3°E (Gulf of Leon)		15/11/90-31/7/91
	36°N, 7°W (Gulf of Cadiz)		15/11/90-31/7/91

which are responsible for variations of a period of a few days observed in our data set.

3. Data

The data of horizontal current velocity, temperature and conductivity of water were taken simultaneously at six different depths by the IEO within the programme "Dynamic study and biological production of the Ibiza Channel" by means of Aanderaa currentmeters, between November, 1990 and July, 1991, interrupted only for a few

days in March to change batteries and tapes of the instruments. The mooring site is marked in Fig. 1 and more details can be found in Table 1.

Meteorological information is available from the Instituto Meteorológico Nacional which consists of series of geostrophic winds in the zone and mean atmospheric pressure over the Gulf of Leon and that of Cádiz, as well as from the Daily Meteorological Reports.

Information from hydrological cruises has also been used. The first cruise took place in November, 1990; the second, in March, 1991. Data from the first one allowed us to plot the Fig. 2. For
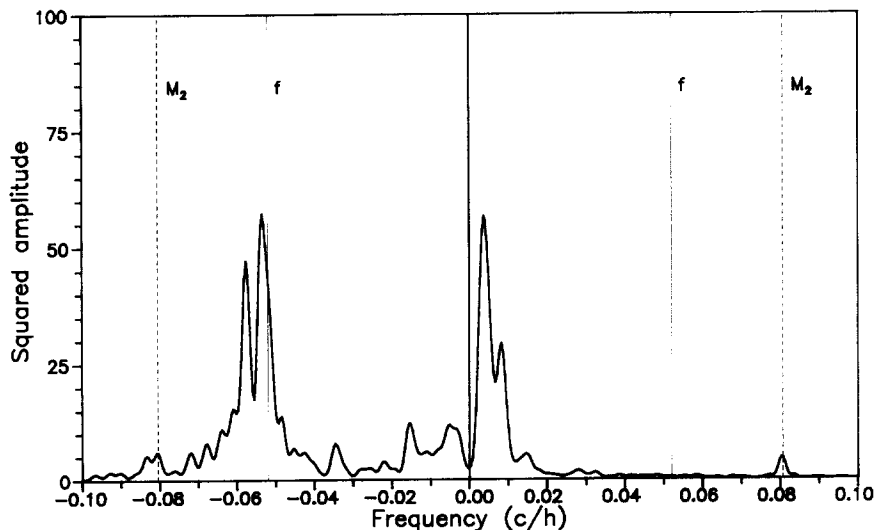

Fig. 3. Rotatory spectrum of the current velocity in depth #2 between November, 1990 and March, 1991. Negative frequencies correspond to clockwise rotation. The very low frequencies ($\sigma < 0.002$ c/h) have been filtered out. Two near-inertial peaks are clearly detected in the clockwise part of the spectrum.
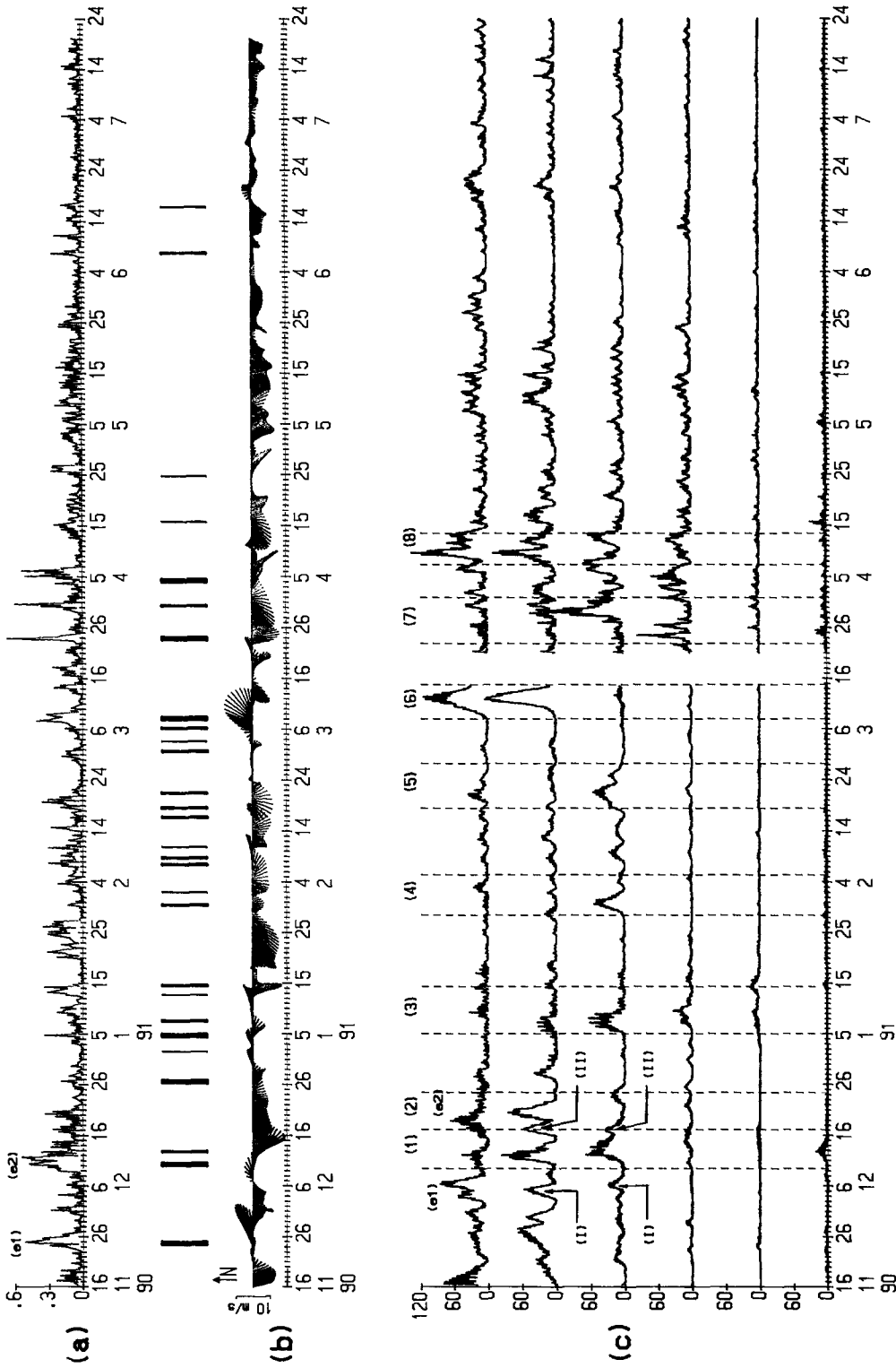
Fig. 4. Modulus of wind-stress (N/m^2) calculated from wind data with a drag coefficient $c_d = 1.5 \ 10^{-3}$. (b) Stick diagram of the low frequency wind velocity. (c) Kinetic energy density (erg/cm^3) of inertial currents in the six sampling depths. Vertical lines between panels (a) and (b) indicate the passage of atmospheric fronts; its thickness is a qualitative measure of its intensity. The different labels which occur in the figure correspond to events discussed in the text.

more information on these hydrological data see Lopez Jurado et al., 1992.

4. Results

4.1. Observations of inertial currents

On all our records of currents, near inertial motions (to which, in short we will call "inertial"), appear persistently, but in an intermittent way. Spectral analysis show that, on average, the peak of energy is located in slightly higher frequencies than f and, sometimes, it appears split (Fig. 3).

To confirm its intermittence, the inertial frequency band has been isolated by complex demodulation of the current velocity. Fig. 4c, which represents the kinetic energy density in the inertial band at different depths, was made from these demodulated series. Usually, the energy decreases with depth but we find some situations in which the uppermost record is not the more energetic one.

Fig. 4a shows the modulus of wind-stress and Fig. 4b the low frequency wind velocity. In this one, the passage of atmospheric fronts has been marked with vertical lines; its thickness represents qualitatively the "strength" of the front. Usually, these fronts come from the N or NW and the associated low pressures pass through the Gulf of Leon, to the north of the mooring site, causing winds of preferentially north component here. They move at speeds between 5 to 15 m/s and are much more frequent and intense in winter. From Fig. 4, as a whole, it is confirmed that to generate inertial waves, the passage of atmospheric fronts is more effective than the existence of a situation of intense but constant winds, circumstance which occurs, for example, between the 19th and 27th of January, 1991.

The detection of inertial waves by our instruments should be delayed with respect to the phenomenon that caused them. For example, the events shown with (e1) and (e2) on the top panel of Fig. 4c could correspond to the passage of the fronts marked (e1) and (e2) also in Fig. 4a. A lagged correlation analysis between both series from the 15th November to the 20th December
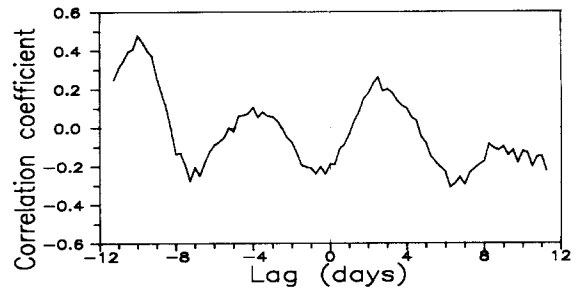

Fig. 5. Lagged correlation between wind-stress and density of kinetic energy of inertial waves in depth #1. Negative lags mean that wind-stress leads inertial currents.

gives significant correlation in minus 10 days (Fig. 5). Assuming that the stratification during these days do not differ from that existing between the 15th to the 20th November, when the hydrological cruise was made, that is, if the mixed layer is ≈ 20 m thick (see Fig. 6), then the inertial waves must have a mean vertical group velocity $c_{gz} = 7$ m/day to arrive at our first instrument (≈ 90 m) from the bottom of the mixed layer.
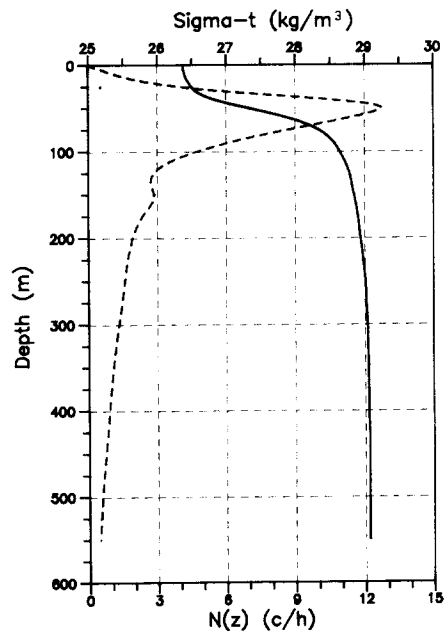

Fig. 6. Profile of sigma-t (solid line) and buoyancy frequency (dashed line) observed near the mooring site during the hydrological cruise of November, 1990.
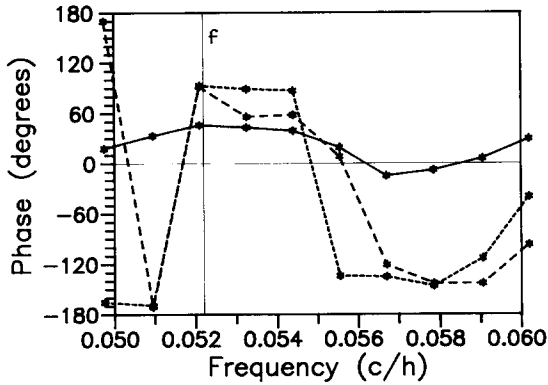
Fig. 7. Inertial band of the clockwise phase spectrum resulting from cross-spectral analysis between currents in depths #1 and #2 (solid line), #1 and #3 (dashed line, short segment) and #2 and #3 (dashed line, long segment) in November – December, 1990. Positive values mean that motion in the lower level leads motion in the upper one. This implies upwards propagation of the phase.
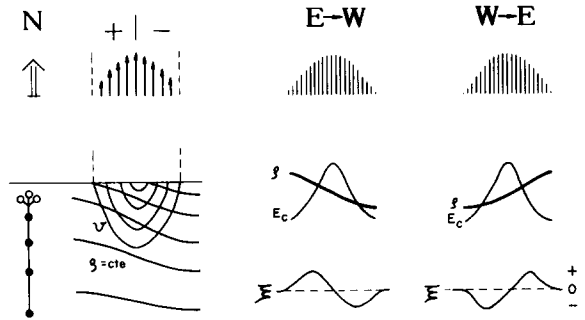

Fig. 8. Signature left by an idealized baroclinic jet and density front, as those represented on the left, when they passes through the mooring site. The upper panel of the figures on the right and center would be the stick diagram for an East to West (center) and West to East (right) displacement of the jet and front. The middle panel, the kinetic energy of the mean flow (thin line) and sigma-t (thick line). The lower panel is the relative vorticity. These signatures would lose identity with depth.

An indirect estimation of c_{gz} can be made from the WKB approximation. According to it and as long as the frequency of the inertial waves, σ, satisfies $f < \sigma \ll N$, N the buoyancy frequency, c_{gz} is given by (Kundu, 1976)

$$c_{gz} = c_z \left[\left(\frac{f}{\sigma} \right)^2 - 1 \right] \qquad (1)$$

where c_z is the "vertical component" of the phase speed. This quantity can be estimated from the clockwise part of the phase spectrum in cross-spectral analysis (see Fig. 7): if $\Delta\theta$ is the phase lag between two currentmeters separated Δz in the vertical, then

$$c_z = \frac{\Delta z}{\Delta\theta} \sigma \qquad (2)$$

which means that if $\Delta\theta > 0$, then $c_z > 0$ (upwards) and, from Eq. (1), $c_{gz} < 0$. This c_z should be understood as a "mean vertical phase speed" between the depths which define Δz and, therefore, c_{gz} calculated with Eq. (1) will be a mean vertical group velocity between those depths. Table 2 summarizes values that permit estimating c_z and c_{gz} from the aforementioned formulas; the product $c_{gz} N$ has also been calculated, resulting approximately constant according to results of the WKB theory in the limit $\sigma \ll N$. Taking an average value $N = 9$ c/h between the base of the mixed layer and the 90 m depth (see Fig. 6) we obtain an average value $c_{gz} = 0.008$ cm/s or 7 m/day. The good agreement of this value with the one obtained before is surprising indeed. Nevertheless, the horizontal inhomogeni-
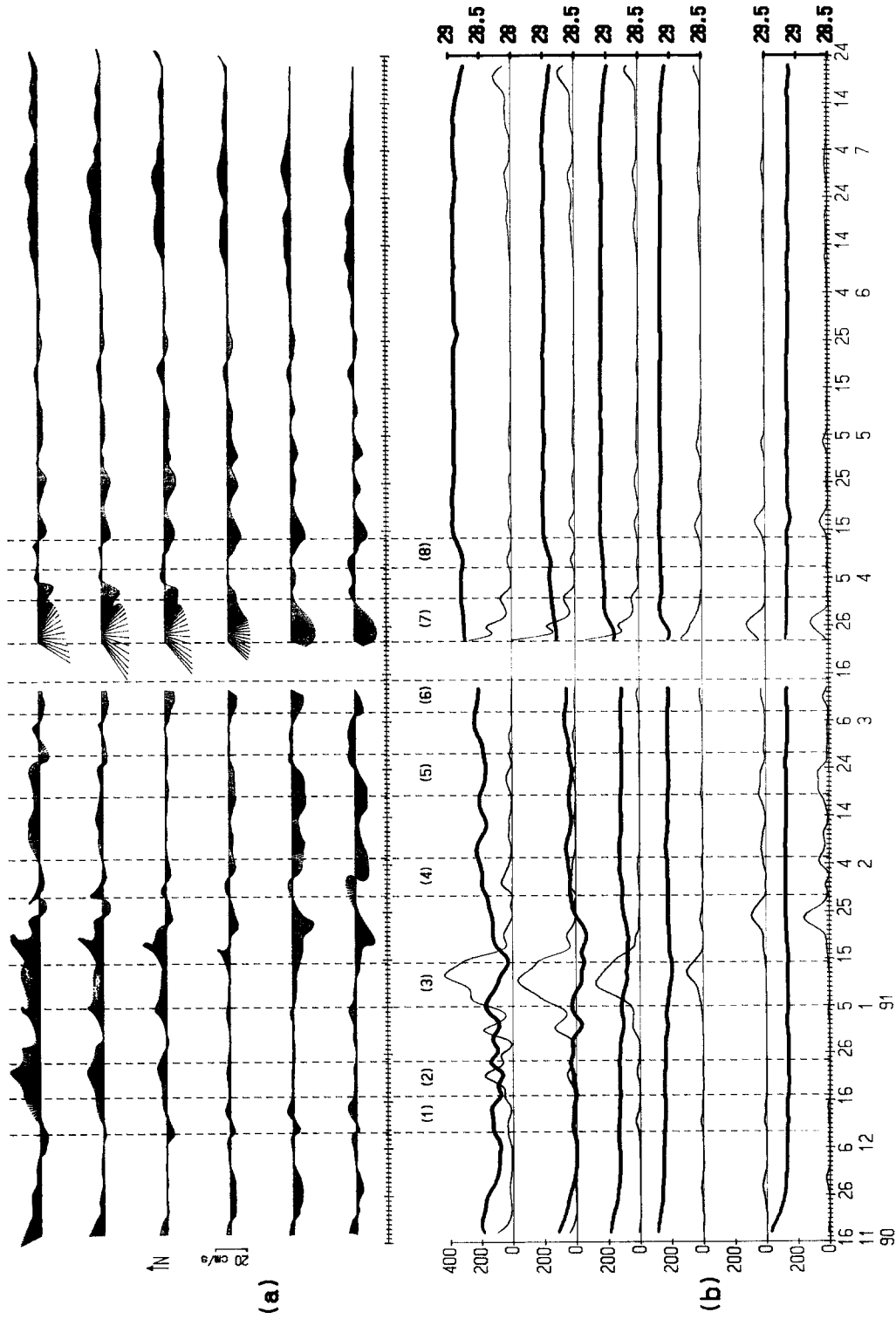
Table 2

Numerical values of some parameters of the inertial waves registered between the 15th of November and the 20th of December, 1990. Values of phase in column 3 have been obtained from results of cross-spectral analysis between the depths shown in column 1 (see Fig. 7 also). Values of N in column 7 (average values between the same depths) are taken from the hydrographic profile shown in Fig. 6. The product $c_{gz} N$, column 8, is constant with considerable approximation, which allows us to estimate c_{gz} if N is known. Thus, for $N = 9$ c/h between 20 and 90 m, results $c_{gz} = 8\ 10^{-3}$ cm/s or 7 m/day, if we accept $c_{gz} N = -0.072$ (cm/s)(c/h).

Depths	Δz (m)	Phase (°)	σ (c/h)	C_z (cm/s)	C_{gz} (cm/s)	N (c/h)	$C_{gz} N$ (cm/s)(c/h)
90–115 m	25	+40°	0.0535	+0.33	−0.016	4.5	−0.072
115–165 m	50	+57°	0.0535	+0.47	−0.023	3.0	−0.069
90–165 m	75	+91°	0.0535	+0.44	−0.021	3.5	−0.074

Fig. 9. (a) Stick diagram of the mean (subinertial) flow in the six sampling depths. (b) Density of kinetic energy of the subinertial flow (erg/cm³, thin line, left scale) and sigma-t (kg/m³, thick line, right scale; there is no information on instrument #5 due to misfunction of the conductivity sensor). The vertical dashed lines and the numbers in brackets refer to concrete events commented in the text.
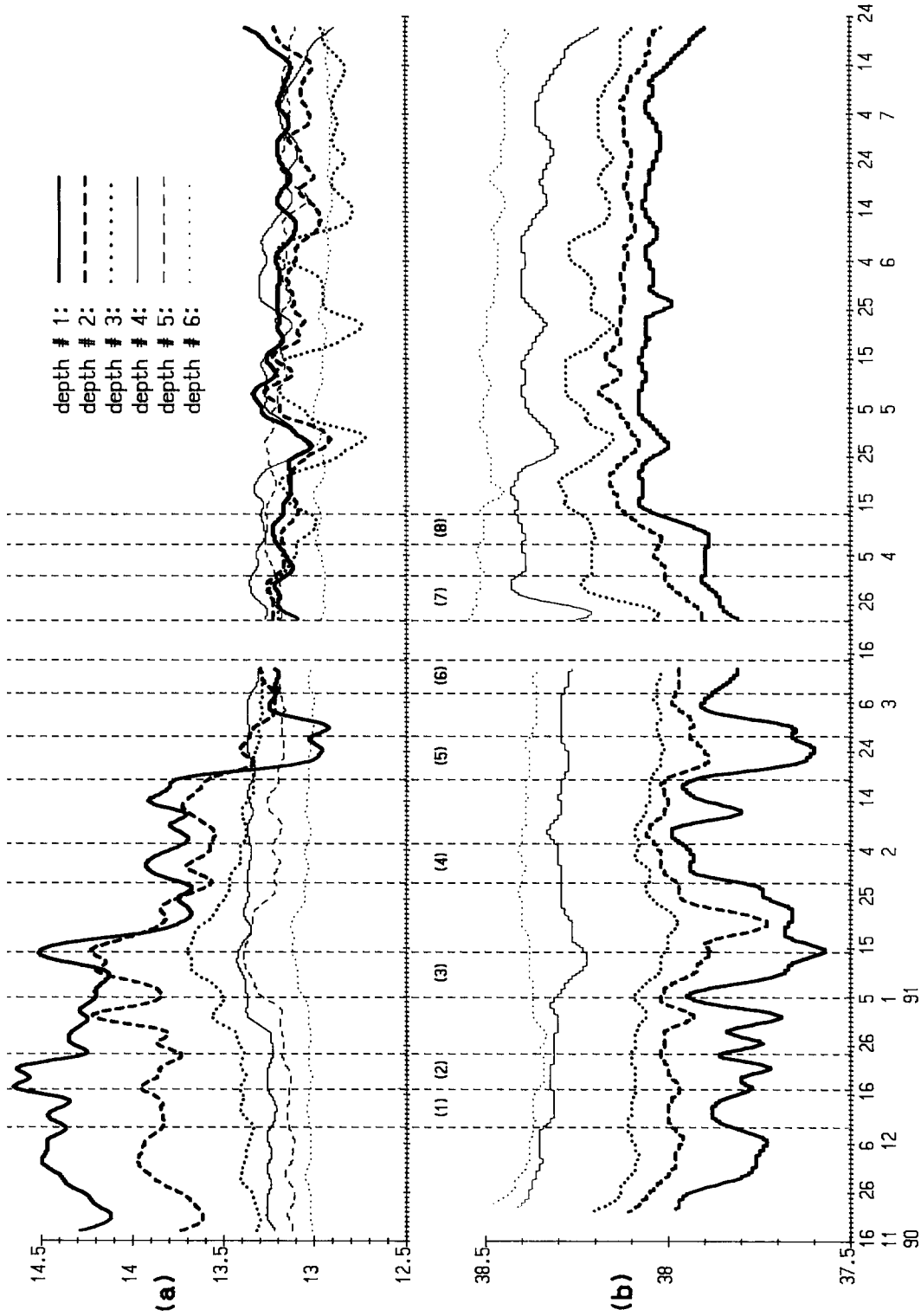
Fig. 10. (a) Time evolution of temperature (°C) in the six sampling depths. (b) Idem for salinity (PSU). Events 1 to 8 have been marked.
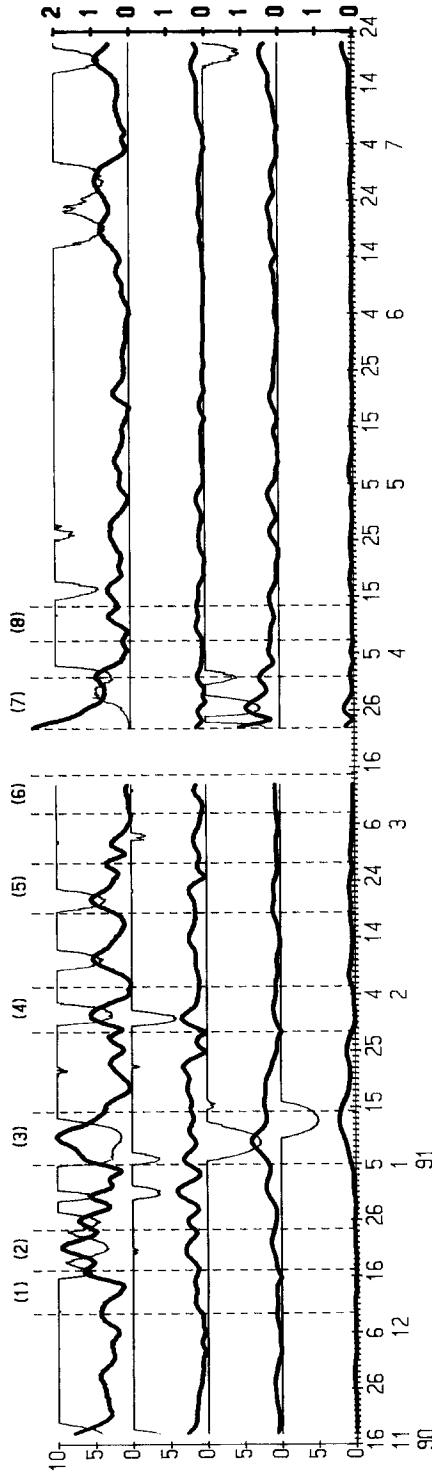
Fig. 11. Averaged Richardson number, Ri, between depths #1 and #2 (first panel), #2 and #3 (second panel), #3 and #4 (third panel) and #4 and #5 (fourth panel) of subinertial flow (thin line, left scale, only $0 < Ri < 10$). The thick line represents the mean vertical shear of subinertial flow (c/h, right scale). It can be seen how low values of Ri are the consequence of strong vertical shears more so than a decrease of $N(z)$.

ties, specifically oceanic fronts, are important in the propagation of inertial waves, as we shall see below.

4.2. Characteristics of the (mean) subinertial flow

With available information only in one position and below the pycnocline, it is not possible to deduce the time evolution of the fields of velocity, density, salinity and temperature (water masses) in the whole region. Fig. 2 shows that these fields could have complex structures. We could infer a certain variability assuming that the mooring site is affected by the fluctuating position of the Balearic Front (which will have drift speed of a few cm/s), and the associated baroclinic jet. This one has instabilities which result in the detachment of eddies or filaments (Wang et al., 1988). Moreover, the long-life mesoscale eddies of LIW, which move westwards from the Strait of Sicily, reported by Millot (1987), can have some influence in the Ibiza Channel: One of them is clearly shown by infrared imagery in Perkins and Pistek, 1990, some ten kms to the south of Ibiza island.

Fig. 8 outlines the signature that an idealized north-flowing baroclinic jet and associated density front would leave on a currentmeter record when it drifts to the west (east) and pass through the mooring site. It can be used to identify some processes shown in Fig. 9, as the arrival or departure of the Balearic Front. Fig. 10 is useful to identify the water masses. The joint study of both gives an idea of the time evolution of the subinertial dynamics which affects the propagation of inertial waves: In certain circumstances, it is responsible for the "easy" downwards penetration of inertial energy and its amplification at a given depth which would correspond to critical layers. There, $c_{gz} \rightarrow 0$ and, consequently, the energy density will increase because of the conservation of the vertical component of the wave action flux, $\langle E \rangle c_{gz} / \sigma$. Finally, this energy will dissipate due to shear instability of the Kelvin–Helmoltz type.

4.3. Inertial waves — mean flow interaction

Henceforth, we shall focuss our attention in the inertial events numbered from 1 to 8 in Figs.

4, 9, 10 and 11. Many of them take place at the same time of some recognisable events of the subinertial flow. The most noticeable of these is simultaneous to event 3 and corresponds to a westwards drift of the Balearic Front, which leaves a clear signature of its passage in the current-meter records. The MAW is found down to depth #3 (165 m) and even #4 (265 m). Fig. 4a indicates the passage of an intense atmospheric front a few days earlier and the combined action of both fronts is undoubtly responsible for the strong penetration of inertial energy observed in Fig. 4c. The pulse of inertial waves which appears in the third depth coincides with the arrival of the oceanic front. Consequently, our mooring would be immersed in a flow of positive relative vorticity (that is, $\xi > 0$). The local effective inertial frequency f_{eff}, defined as (see Mooers, 1975)

$$f_{eff} = [f(f + \xi)]^{1/2} \approx f + \tfrac{1}{2}\xi \qquad (3)$$

(where the second equality stands for $\xi \ll f$, as usually occurs in the actual oceanic flows) is greater than f. Inertial waves propagating eastward would encounter a "vorticity wall": its frequency would be less than f_{eff} on the boundary of the jet and would not be able to propagate much further, having to reflect back. This reflection will facilitate the penetration and dispersion of energy towards the bottom of the sea (Kunze, 1985; Wang, 1991) or its eventual dissipation due to the increase of the vertical shear.

Event 2 fulfils similar characteristics. As a matter of fact, the first clear intrusion of the Balearic Front occurs about the 16th or 17th of December. Since then until the end of January the MAW is detected on the most superficial currentmeters.

Events 1 and 4 are of a different nature. Fig. 10 shows an increase of salinity in the upper records due to a greater presence of LIW. The stick diagram on Fig. 9 confirms the passage of a structure (mesoscale eddy?) which affects the column of water up to 90 m, especially during event 4. The time series of temperatures and salinities (Fig. 10) show how this water reach the depth #1 about the 28th of January, forcing the Balearic Front to withdraw or to confine itself to a more

superficial layer. Anyhow, it remains out of our instruments. By these days several atmospheric fronts, not very intense, passed over the Channel. On January 29, we observe the appearance of a sequence of pulses of inertial waves with remarkable amplitude at depth #3. However, high values of subinertial velocity are not observed; the field velocity rather appears as a two-layer baroclinic flow with zero-crossing in the vicinity of this depth.

This appearance maintains itself until event no. 5. This, as no. 8, corresponds to the arrival of WMIW. The arrival was clearly detected at depth #1 (see Fig. 10) but, again, the subinertial current did not have high values nor sudden changes of intensity, which we could identify with movements of the Balearic Front. Weak atmospheric fronts continue passing but the apparent absence of an oceanic front complicates the interpretation of the energetic inertial event in depth #3 in terms of mean flow − inertial waves interaction.

Event no. 7 corresponds to the withdrawal of WMIW from depths #3 and #4. One does notice the presence of an oceanic front or similar feature (the lack of data between 14th and 23th of March does not help to understand the energetic feature observed during the first days of the second mooring) which, again, seems to move westwards. As the jet flows to the south now, the currentmeters would remain in a negative relative vorticity trough ($\xi < 0$ and $f_{eff} < f$) at the beginning of the withdrawal, which could result in the trapping of inertial waves in this trough (Kunze, 1985). Likely, this was the cause of the strong and persisting presence of inertial energy at 250 m during those days, circumstance which, on the other hand, was not repeated again.

5. Discussion

The relation found between the passage of atmospheric fronts and the appearance of inertial motions allows to prove the effectiveness of those as generating forces of this waves. The theory of generation and downwards propagation of these perturbances as a set of internal modes predicts that their frequencies should be slightly greater than the local inertial one, as occurs in our observations.

Sometimes and only in certain depths, a double peak appears in the spectrum. This occurs, for example, in depths #2 (Fig. 3) and #3 (not shown) during December, 1990. The WKB approximation gives good results when applied to the peak nearest to f, $\sigma_1 = 0.0535$ c/h. However, the results obtained for the other peak of larger frequency, $\sigma_2 = 0.0580$ c/h, have a more difficult interpretation: depths #2 and #3 are $\Delta z = 50$ m apart and, from Fig. 7, $\Delta \theta = -140°$, which gives $c_z = -2 \ 10^{-3}$ m/s and $c_{gz} = +4 \ 10^{-4}$ m/s ≈ 35 m/day between those depths. This upwards propagation could be explained by a lateral reflection of downgoing inertial waves with such an angle that the inclination of the incident ray, α_1, exceeds that of the continental slope, α_2 (Leblond and Mysak, 1978). The latter is, on average, $\alpha_2 = 0.02$ and the former is given by $\alpha_1 = k_h/k_z$ where k_h and k_z are the horizontal and vertical components of the wavenumber vector. The WKB approximation establishes the relationship (see Kundu, 1976)

$$k_z^2 = k_h^2 \frac{N^2 - \sigma^2}{\sigma^2 - f^2} \qquad (4)$$

which gives $k_h/k_z (= \alpha_1) = (\sigma^2 - f^2)^{1/2} N^{-1}$ in the limit $\sigma \ll N$. Within the first 250 m, excluding the upper mixed layer, $N > 2$ c/h and $\alpha_1 < 0.01 < \alpha_2$. Therefore, a lateral reflection with sign inversion in c_{gz} is not possible. Moreover, since the inertial motion is circular, the instantaneous phase can be estimated from $\tan^{-1}(u/v) = \sigma t + \theta_0$ where u and v are the eastward and northward components of the velocity and θ_0 an arbitrary constant that depends on our choice of $t = 0$. Thus, σ is the slope of $\tan^{-1}(u/v)$ against t. This result allows us to estimate the frequencies of the different wave packets appearing in Fig. 4c and identify those of $\sigma_2 = 0.0580$ c/h, which have been marked by arrows. Their situation in the figure and their intensity do not suggest upwards propagation at all! The WKB approximation fails to explain this peak.

A more acceptable explanation is that those wave packets have been generated in a place

where the effective inertial frequency f_{eff} equals σ_2, that is, in a place of positive relative vorticity, and they progress having the shape of a vertical internal mode. The value $\Delta\theta = 140°$, phase difference between 115 and 165 m, close to 180°, supports this assumption. Moreover, packet (ii) in Fig. 4c coincides with event number 2, the arrival of the Balearic Front (westwards drift of it, indeed) and, from Fig. 8, f_{eff} must be greater than f by the surroundings of the mooring site. The structure of the baroclinic jet associated with the Front will not be very different from that shown in Fig. 2d and the relative vorticity would be $\xi = \Delta v/\Delta x \approx 1.5$ cm/s/km ≈ 0.01 c/h. Substituting this value in Eq. (3), we obtain $f_{eff} = 0.0572$, very close to σ_2. If inertial waves coming from places with different local vorticity are detected by our instruments, it is not surprising to find the peak splitting. Another example is found during the first days of the second mooring in depths #3 and #4. Then, the instruments are immersed in a negative relative vorticity trough ($f_{eff} < f$) and the spectral analysis also shows a double peak with one of the frequencies slightly smaller than f.

Assuming that the subinertial flow is in geostrophic balance, the horizontal density inhomogenities due to the presence of the fronts influence the vertical shear via the "thermal wind" relation. The Richardson number, defined as

$$Ri = \frac{N^2}{\left(\dfrac{\partial u}{\partial z}\right)^2 + \left(\dfrac{\partial v}{\partial z}\right)^2} \tag{5}$$

is a measure of stability against vertical shear. $Ri < 1$ favours instability and the flow becomes unstable if $Ri < 0.25$. Fig. 11 is a plot of vertical shear (square root of the denominator of Eq. 3) and of Ri of the subinertial flow, estimated from our data. Of course, they will have to be understood as averaged values between the depths which permit their estimation.

The simultaneity of high values of inertial energy in depth #3 (Fig. 4c) and low values of Ri is surprising. Actually, $Ri < 0.25$ during event no. 7 between depths #1 and #2. Likely, this is a

reason for the low level of inertial energy between these depths, as internal breaking and dissipation will be favoured.

Another possible episode of internal breaking would be event no. 6. The subinertial flow does not reflect energetic features nor does Fig. 10 show the arrival of any water mass by those days. Apparently, we deal with a phenomenon of free propagation of inertial waves, without interaction with the mean flow. These waves could have been excited at the Spanish coast by the atmospheric front which passed the 7–8 of March (Fig. 4), progressing eastward from there in the wake of the front. In accordance to Fennel (1989), the horizontal group velocity c_{gh} is given by

$$c_{gh} = c_n\left(1 - \frac{f^2}{\sigma^2}\right)^{1/2} \tag{6}$$

where c_n is the phase speed of mode n. With the $N(z)$ profile of Fig. 6, the first baroclinic mode has $c_1 = 0.51$ m/s. Taking $\sigma = 0.054$ c/h (see later), we obtain $c_{gh} = 11$ km/day and about three days would be necessary to get the mooring site from the Cape "La Nao", next to point A in Fig. 1. This result is compatible with the delay between the front passage and the full development of inertial event 6 observed in Fig. 4.

Fig. 12a and b represent the u-component of the velocity (from both original and demodulated series). Motion in depth #1 develops a short time before than in depth #2. When it reaches this one, a phase shift begins to be produced because of frequency in depth #2 is slightly greater than in depth #1: a least square fit of $\tan^{-1}(u/v)$ against t during the period of Fig. 12 gives 0.0531 c/h and 0.0544 c/h for the mean frequencies in depths #1 and #2 respectively. If we fit the pieces one inertial period long, we can obtain a smoothed time dependence of $\sigma_{\#1}$ and $\sigma_{\#2}$ with time. Fig. 13 shows the difference $\sigma_{\#2} - \sigma_{\#1}$ together with the accumulated phase shift. The difference diminishes with time and most of the phase shift occurs at the beginning of the pulse, when $\sigma_{\#2} - \sigma_{\#1}$ is high. This behaviour recalls the propagation of a set of internal modes that have been remotely excited (likely, at the coast): once the perturbation arrives at a given point, the

local frequency decreases with time [see, for example, Gill (1984) or Fennel (1989) for more details]. The progressing wave packet reaches depth #1 a little before; when it reaches the second one, frequencies must differ in both depths at a given time, being greater in the latter. Subsequently, they tend to equalize but the phase difference is kept, leading to strong vertical shear. The Richardson number of the whole flow takes very low values because of the contribution of the "inertial" part (subinertial shear is negligible, see Fig. 11). Values even below the stability limit are found (Fig. 12c) and internal breaking is favoured, preventing the energy from penetrate deeper. Local vertical progression of the waves stops in the vicinity of depth #2 and they do not get
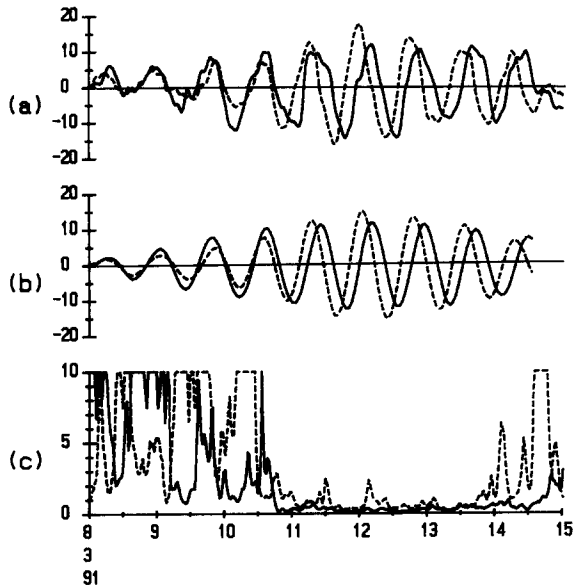

Fig. 13. (a) Difference of frequencies between depths #2 and #1, $\sigma_{\#2} - \sigma_{\#1}$, during event 6 [solid line, scale on the left (c/h × 100)]. (b) Phase difference between the same depths [dashed line, scale on the right (degrees)]. An arbitrary phase origin has been chosen at the beginning of the plot, that is, 9th of March at 12:00, when the inertial waves are well developed in both depths, according to Fig. 12. The difference of frequencies is greater at the beginning of the pulse and then decreases to 0, while the difference of phase increases to finally reach an almost constant value around 100°.

Fig. 12.(a) E–W component of the velocity (cm/s) taken from the original series in depths #1 (solid) and #2 (dashed line) during event 6. (b) Complex demodulated version of (a). In both it can be observed how the near-inertial period in depth #2 is slightly shorter than in depth #1 at the beginning of the pulse. This results in the leading of the inertial currents in depth #2 with reference to depth #1. Although the periods are equalled later, the lag is maintained and strong vertical shears are developed. Consequently, we find very low Ri values, even below the limit of stability from 11th to 14th of March, as (c) shows. On it, Ri of the whole (inertial plus subinertial) flow between depths #1 and #2 (solid line), and #2 and #3 (dashed line) is represented.
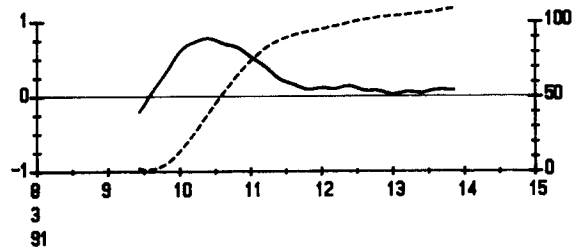
depth #3 (see Fig. 4). The vertical energy flux arriving at the second depth is about 8 J/m³ × 2 10^{-4} m/s = 1.6 mW/m² (energy density times c_{gz}). This value agrees with the rate at which energy should be extracted from a volume of unit surface and height H, H being the distance between depths #1 and #2, in order to remove all the energy in the decaying time observed in Fig. 4c, i.e., 2 days. In other words, $\frac{1}{2}\rho u_i^2 H t^{-1} = 1.7$ mW/m². It is important to say that these episodes of internal breaking do not appear to be the rule.

A question to be answered is the existence of inertial energy in certain depths when it is hardly detected in more superficial instruments on the same date. For example, what happens with events 4 or 5. Some possible explanations exist: (1) Waves generated somewhere on the surface and propagating downwards may interact with the mean flow and reach a critical layer in the vicinity of the depth concern. As they approach it, c_{gz} decreases and the conservation of the vertical component of the wave action flux would imply an $\langle E \rangle$ increase. Such a possibility is analyzed in Kunze (1985), but all this must occur in a trough of negative relative vorticity and this does not seem to be our case; (2) the energy comes laterally in a very directional way from some remote place having the shape of an internal mode with a zero-crossing above this depth.

Eventual advection by the subinertial flow may contribute to the horizontal propagation of the waves. This is partially supported by our data set as a different water mass is detected above depth #3 coming from the south during events 4 and 5 (see Figs. 9 and 10) and (3) the waves are generated in the interior, near of that depth, as transients during geostrophic readjustments. This hypothesis has been mentioned by some authors (Tang, 1979) and analyzed by Kunze and Sanford (1984) in terms of energy transfer from subinertial to inertial flow. Near of oceanic fronts and in superficial layers the subinertial flow usually has enough kinetic or/ and potential energy to excite inertial waves, transferring energy to them. In our case, such a transfer of energy is also possible. However, it is important to note that this cause has never been verified. Our data does not allow us to choose one of them as they do not resolve the horizontal structure of the inertial waves and mean flow fields nor the motions in the mixed layer. Any conclusion will be unavoidably speculative. Perhaps cause 2 is the most convincing.

Acknowledgements

References

D'Assaro, E.A., 1985. The energy flux from the wind to near-inertial motions in the surface mixed layer. J. Phys. Oceanogr., 15: 1043-1059.

Eriksen, C.C., 1988. Variability in the upper-ocean internal wave field at a Sargasso site. J. Phys. Oceanogr., 18: 1495-1513.

Fennel, W., 1989. Inertial waves and inertial oscillations in channels. Cont. Shelf Res., 9: 403-426.

Font, J., 1986. La circulación general del Mar Catalán. Ph.D. Thesis, Barcelona University, 323 pp.

Gill, A.E., 1984. On the behaviour of internal waves in the wakes of storms. J. Phys. Oceanogr., 14: 1129-1151.

Kundu, P.K., 1976. An analysis of inertial oscillations observed near Oregon coast. J. Phys. Oceanogr., 6: 879-893.

Kundu, P.K. and Thomson, R.E., 1985. Inertial oscillations due to a moving front. J. Phys. Oceanogr., 15: 1076-1084.

Kunze, E., 1985. Near-inertial wave propagation in geostrophic shear. J. Phys. Oceanogr., 15: 544-565.

Kunze, E. and Sanford, T.B., 1984. Observations of near-inertial waves in a front. J. Phys. Oceanogr., 14: 566-581.

La Violette, P.E., Tintore, J. and Font, J., 1990. The surface circulation of the Balearic Sea. J. Geophys. Res., 95: 1559-1568.

LeBlond, P.H. and Mysak, L., 1978. Waves in the Ocean. Elsevier Oceanographic Series, New York, 602 pp.

Levovrh, J. et al., 1992. Atlas des fronts thermiques en Mer Mediterranèe d'apres l'imagerie satellitaire. Mem. Inst. Oceaonogr., 16, 146 pp.

Lopez Garcia, M.J., 1991. La temperatura del Mar Balear a partir de imágenes de satélite. Ph.D. Thesis, Valencia University, 158 pp.

Lopez Jurado, J.L. et al., 1992. Resultados preliminares de la campaña IBIZA-90. Inf. Tecn. Inst. Esp. Oceanogr., 113, 55 pp.

Millot, C., 1987. The circulation of the Levantine Intermediate Water in the Algerian Basin. J. Geophys. Res., 92: 8265-8276.

Mooers, C.N.K., 1975. Several effects of a baroclinic current on the cross-stream propagation of internal-inertial waves. Geophys. Fluid Dyn., 6: 245-275.

Perkins, H. and Pistek, P., 1990. Circulation in the Algerian Basin during June 1986. J. Geophys. Res., 95: 1577-1585.

Rubinstein, D.M. and Roberts, G.O., 1986. Scattering of inertial waves by an ocean front. J. Phys. Oceanogr., 16: 121-131.

Tang, C.L., 1979. Inertial waves in the Gulf of Saint Lawrence. A study of geostrphic adjustment. Atmos. Ocean., 17: 135-156.

Wang, D.P., 1991. Generation and propagation of inertial waves in the subtropical front. J. Mar. Res., 49: 619-633.

Wang, D.P. et al., 1988. A shelf/slope filament off the Northeast Spanish coast. J. Mar. Res., 46: 321-332.

Weller, R.A., 1985. Near-inertial velocity variability at inertial and subinertial frequencies in the vicinity of the California Current. J. Phys. Oceanogr., 15: 372-385.

Weller, R.A. et al., 1991. Forced ocean response during the Frontal Air-Sea Interaction Experiment. J. Geophys. Res., 96: 8611-8638.